AT&T Technical Journal
Vol. 64, No. 1, January 1985
Printed in U.S.A.

Effects of Channel Impairments on the Performance of an In-band Data-Driven Echo Canceler

By J. J. WERNER*

(Manuscript received July 11, 1984)

High-speed (≥ 4.8 kb/s) echo-cancellation-based full-duplex direct distance dialing modems usually have to deal with two echos: the near echo, which is generated at the modem location, and the far, or talker, echo, which has been looped back to the modem after passing through a carrier system. The near echo propagates through a channel that is essentially linear, and thus it can, at least in theory, be perfectly canceled by an echo canceler. On the other hand, the far-echo channel is generally plagued by impairments that can seriously degrade the performance of an echo canceler. In this paper we study the effects of these channel impairments on the performance of an in-band data-driven echo canceler. This echo canceler has been found to be particularly well suited for full-duplex voice-grade data transmission applications. Both analytical and real-time experimental results are presented. It is shown that frequency offset, even in small amounts, is by far the most damaging of the channel impairments that are commonly encountered in carrier systems. The degradation of performance due to phase jitter can be significant. However, this can only happen under simultaneous worst-case conditions of phase jitter and signal power levels, and these cases might not be statistically significant. Worst-case nonlinearities in the echo channel do not degrade substantially the performance of the echo canceler.

I. INTRODUCTION AND SUMMARY

In this paper we study the effects of channel impairments on the performance of a data-driven in-band echo canceler. This echo can-

* AT&T Information Systems, Inc.

celer is intended to be used in two-wire, high-speed (≥ 4.8 kb/s), full-duplex, voice-grade data transmission. Details about this application for 4800 b/s Direct Distance Dialing (DDD) operation are given in Ref. 1. Performance degradations due to finite precision effects in the digital implementation of the echo canceler are studied in a companion paper.[2]

The use of echo cancellation in two-wire, full-duplex data transmission will be described with reference to Fig. 1.[3-6] Figure 1a shows a simplified version of a typical connection over the switched network. Echoes arise because of impedance mismatches in the hybrid couplers that make the connections between two-wire and four-wire transmission facilities. Consequently, some energy leaks directly through the first hybrid encountered by the transmitted signal. This signal is called the *near echo*. Similarly, some energy leaks through the hybrid at the other end of the four-wire circuit and is looped back to the modem through the carrier system. This signal is called the *talker* or *far echo*. These two echoes are added to the signal transmitted by the far-end modem, and they appear as interference at the receiver's input.

The echo canceler in Fig. 1b synthesizes a replica of the channel traversed by the echoes. It can take its input from various points of the transmitter. For example, a voice-type canceler takes its input from the output of the transmitter, whereas a data-driven canceler gets its input directly from the data symbols at the input of the transmitter. Under ideal conditions, if the canceler and the echo channel have the same inputs, they should also have the same outputs,

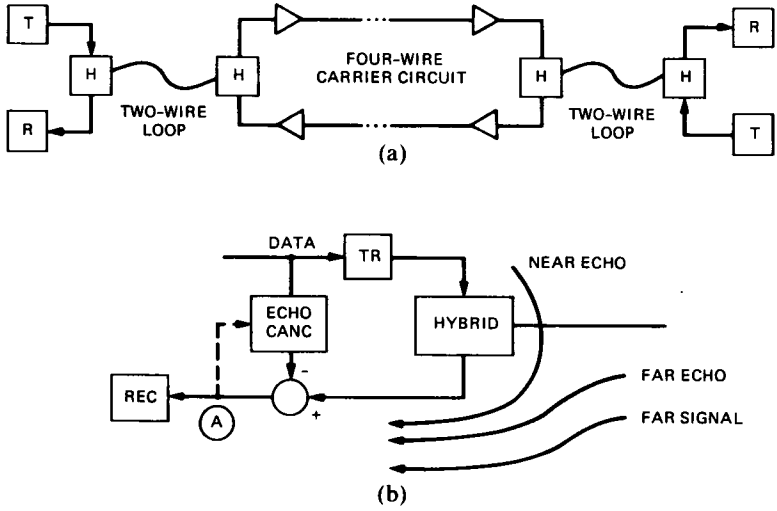

Fig. 1—(a) Typical dialed connection. (b) Use of data-driven echo canceler at station location.

and the signal, after subtraction at point A, should consist only of the wanted far-end data signal. These ideal conditions exist, to some extent, for the near-end echo because the hybrid introduces mainly linear distortion (for which the canceler can compensate perfectly if its memory span and the digital precision are large enough). However, this is not true for the far echo that has propagated through a channel that is generally time varying and nonlinear. The updating algorithms and structure used in the basic canceler can only compensate partially, if at all, for these impairments, and some residual echo will appear at point A in Fig. 1b. Some of the effects of these channel impairments for voice-type cancelers are studied in Refs. 7 through 11.

Because the near echo and the far echo have different characteristics, we will find it convenient to break the canceler into two parts, a near canceler and a far canceler. The requirements for these two cancelers are quite different. Due to the delay characteristics of the far-echo channel, the far canceler requires a larger memory span than the near canceler. However, under worst-case conditions of hybrid leakage and signal levels, the near canceler has to provide a much larger echo attenuation than the far canceler. In both cases these attenuations generally have to be achieved under "double-talking"* (full-duplex transmission) conditions and, in the case of the far canceler, in the presence of time-varying and nonlinear echo-channel impairments.

Our purpose in this paper is to study the performance degradation of the far canceler in the presence of the impairments that are most commonly encountered in carrier systems. The echo canceler used in the study is the so-called data-driven, Nyquist, in-band canceler. Its structure is derived in the next section. The experimental and analytical work presented here consisted of studying the signals at point A, in Fig. 1b, when different types of impairments were inserted in the far-echo channel. In the experimental setup, the echo channel was simulated by using the appropriate laboratory equipment, and real-time performance measurements were achieved by using an echo canceler implemented on an in-house developed digital signal processor. We now summarize our findings. Frequency offset, even in small amounts (a fraction of a hertz), is found to be the most damaging of all the impairments. Possible corrective actions are studied in a forthcoming paper. The performance of the canceler can also be significantly degraded by phase jitter. However, in practice, this can

* The signal at point A in Fig. 1b is used to adapt the echo canceler's tap coefficients. In steady-state operation this signal will consist mostly of the far signal, which will thus act as a strong noise component in the adaptation algorithm.[10] An arrangement proposed recently allows, in principle, the elimination of the double-talker from the adaptation algorithm.[12]

only happen under certain simultaneous worst-case (round-trip) conditions of jitter and signal power levels, and these cases might not be statistically significant. Worst-case nonlinearities did not degrade substantially the performance of the canceler.

The paper is organized as follows. The structure of the echo canceler used in this study is derived in the next section. Its convergence properties in the presence of a double-talker are analyzed in Section III. The effects of phase jitter and frequency offset are studied in Sections IV and V, respectively. Finally, in Section VI we present real-time performance results obtained with an echo canceler implemented on a bit-slice processor.

II. IN-BAND ECHO CANCELER STRUCTURE

The echo canceler structure derived in this section is of the Nyquist or interpolating type. That is, it cancels the echo at all frequencies. It is also called an in-band canceler because it synthesizes passband filters rather than equivalent baseband filters. This canceler is particularly attractive because it is less complex to implement than either the voice-type canceler or the Nyquist data-driven canceler described in Ref. 6.

A two-dimensional (in-phase and quadrature) modulated signal is generally represented by the expression

$$s(t) = \mathrm{Re}\left\{\sum_n A_n g(t - nT)e^{j\omega_c t}\right\}, \tag{1}$$

where $A_n = a_n + jb_n$ is the discrete-valued multilevel complex symbol to be transmitted, $g(t)$ is a Nyquist pulse, $1/T$ is the symbol rate, and $\omega_c/2\pi$ is the carrier frequency. In the usual case where the highest frequency component in $g(t)$ is smaller than the carrier frequency, the complex signal in brackets in (1) is an analytic signal $Z(t)$, where

$$Z(t) = s(t) + j\tilde{s}(t) = \sum_n A_n g(t - nT)e^{j\omega_c t}, \tag{2}$$

and where $\tilde{s}(t)$ is the Hilbert transform of $s(t)$. Equation (2) can be rewritten as

$$Z(t) = \sum_n A_n e^{j\omega_c nT} g(t - nT)e^{j\omega_c (t-nT)} \tag{3}$$

$$Z(t) = \sum_n A'_n R(t - nT), \tag{4}$$

where

$$A'_n = A_n e^{j\omega_c nT} \tag{5}$$

$$R(t) = g(t)e^{j\omega_c t}. \tag{6}$$

When the signal $s(t)$ is transmitted through a channel with impulse response $h(t)$, the analytic signal corresponding to the output signal is

$$Z_1(t) = Z(t)*h(t) = \sum_n A'_n R_1(t - nT), \tag{7}$$

where * denotes convolution and

$$R_1(t) = R(t)*h(t), \tag{8}$$

and where $Z_1(t)$ and $R_1(t)$ are analytic signals. The signal at the output of the channel is the real part of $Z_1(t)$, i.e.,

$$s_1(t) = \sum_n [a'_n r_1(t - nT) - b'_n \tilde{r}_1(t - nT)], \tag{9}$$

where $R_1(t) = r_1(t) + j\tilde{r}_1(t)$.

Thus, the echo $s_1(t)$ is obtained by feeding the symbols a'_n and b'_n to in-phase and quadrature bandpass filters with impulse responses $r_1(t)$ and $\tilde{r}_1(t)$, respectively. This suggests the following structure for a digitally implemented data-driven echo canceler. We can feed the rotated symbols a'_n and b'_n to two transversal filters with variable tap coefficients and tap delay spacings of T'. The signal $s_1(t)$ in (9) is sampled at a rate $1/T'$, which will be assumed to be at least twice the highest frequency of $s_1(t)$, so that the wanted far signal, which is added to $s_1(t)$ in full-duplex operation, can be reconstructed after cancellation. A standard Mean-Squared Error (MSE) criterion can then be used to adapt the tap coefficients. Ideally, after adaptation, the tap coefficients of the two transversal filters converge to the sampled values of $r_1(t)$ and $\tilde{r}_1(t)$ in (9). The echo canceler structure is shown in Fig. 2. Notice from (4), (5), and (6) that the same structure can be used to implement the transmitter, in which case the tap coefficients are fixed.[13]

Referring again to Fig. 2, the transmitter generates the symbols a'_n and b'_n at the symbol rate $1/T$, which is always smaller than the sampling rate $1/T'$. Therefore the canceler's delay lines in Fig. 2 will only be sparsely filled. In fact, they will contain $L - 1$ zeros for each

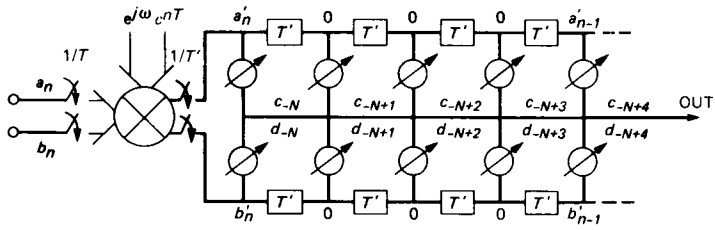

Fig. 2—In-band data-driven echo canceler structure.

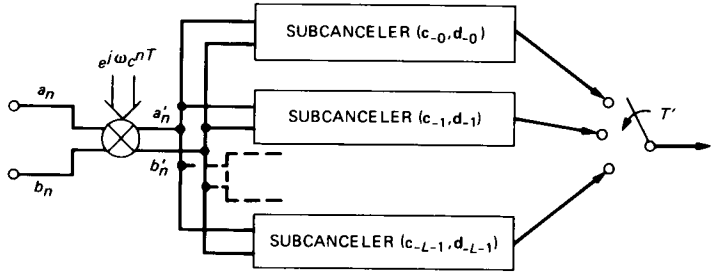

(a)

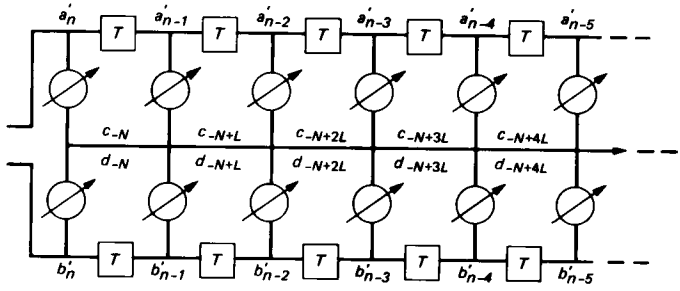

(b)

Fig. 3—(a) Modified canceler structure. (b) Subcanceler structure.

nonzero symbol, where $L = T/T'$ is the number of sampling periods per symbol interval.* A direct implementation of this canceler structure would waste computation power since multiplication by zero need not be performed. A more efficient, but equivalent, structure can be derived by observing that a different subset of coefficients is used for the computation of the output when the symbols move down the delay line in Fig. 2. There are L such subsets that are each used once per symbol interval. All the subsets of coefficients are correlated with the same input vectors $(a'_n, a'_{n-1}, \cdots)$ and $(b'_n, b'_{n-1}, \cdots)$ in a given symbol period. Therefore the canceler can be considered as a parallel combination of L "subcancelers" having all the same delay line but different sets of coefficients, as shown in Fig. 3a. One of the subcancelers is shown in Fig. 3b. The taps of the transversal filters are now spaced at T rather than T', and none of the entries in the delay lines are zero. The ith subcanceler consists of the tap vectors $\mathbf{c}_i$ and $\mathbf{d}_i$ whose elements

* Theoretically many other interpolation schemes can be envisioned. However, the scheme described here leads to the simplest possible practical implementation of the echo canceler.

are $c_{-N+i+kL}$ and $d_{-N+i+kL}$, respectively, where $i = 0 \cdots L - 1$. The outputs of the canceler are generated at the sampling rate $1/T'$ by computing, in a cyclic fashion, the outputs of the L subcancelers shown in Fig. 3a. This model applies also to the echo channel and we can consider that it consists of a parallel combination of L subchannels. Convergence of the whole canceler can then be achieved by having each subcanceler converge to the corresponding subchannel. The algorithms used during adaptation are described in the next section.

III. CONVERGENCE PROPERTIES IN THE PRESENCE OF A DOUBLE-TALKER

In order to adapt the tap coefficients of the canceler, we will separately minimize the MSE between the outputs of each subcanceler and the corresponding echo subchannel. That is, each subcanceler's output is computed once per symbol interval, an error is derived, and a stochastic-gradient algorithm is used to update the tap coefficients. Nyquist cancellation is obtained by cyclicly repeating these operations at the sampling rate $1/T'$ for all the subcancelers. We analyze this adaptation scheme by assuming that the subcancelers adapt independently. This assumption was found to be in excellent agreement with our experimental results. For simplicity of notation, we will also assume that the inputs of the echo canceler are the original symbols a_n and b_n rather than the rotated symbols a'_n and b'_n. We now define the following quantities, at the nth symbol instant:

$\mathbf{a}_n^T = [a_n, a_{n-1}, a_{n-2}, \cdots]$ = in-phase data vector.

$\mathbf{b}_n^T = [b_n, b_{n-1}, b_{n-2}, \cdots]$ = quadrature data vector.

$\mathbf{c}_i^T = [c_{-N+i}, c_{-N+i+L}, c_{-N+i+2L}, \cdots]$

= vector of in-phase tap coefficients of ith subcanceler.

$\mathbf{d}_i^T = [d_{-N+i}, d_{-N+i+L}, d_{-N+i+2L}, \cdots]$

= vector of quadrature tap coefficients of ith subcanceler.

$\mathbf{r}_{1i}^T = [r_1(iT'), r_1(T + iT'), r_1(2T + iT'), \cdots]$

= vector of in-phase samples of ith echo subchannel.

$\mathbf{r}_{2i}^T = [r_2(iT'), r_2(T + iT'), r_2(2T + iT'), \cdots]$

= vector of quadrature samples of ith echo subchannel.

The superscript T designates transposed vectors where all these vectors are assumed to be infinite. For finite-length cancelers shorter than the echo-channel impulse response, we simply insert zeros on the right in the definitions of $\mathbf{c}_i^T$ and $\mathbf{d}_i^T$. The outputs, $s_e(nT + iT')$ and

$s_c(nT + iT')$, of the ith subchannel and the ith subcanceler at time $nT + iT'$ are

$$s_e(nT + iT') = \mathbf{a}_n^T \mathbf{r}_{1i} + \mathbf{b}_n^T \mathbf{r}_{2i} + \xi_{n,i} \tag{10}$$

$$s_c(nT + iT') = \mathbf{a}_n^T \mathbf{c}_i + \mathbf{b}_n^T \mathbf{d}_i, \tag{11}$$

where $\xi_{n,i}$ is an additive interference signal that is uncorrelated with the signal to be canceled. This interference will generally consist of the desired (far-end) data signal and some additive noise. The error $e_{n,i}$ between the outputs of the ith subchannel and the ith subcanceler is

$$e_{n,i} = s_e(nT + iT') - s_c(nT + iT'), \qquad i = 0, 1, \cdots, L - 1, \tag{12}$$

and we want to minimize the MSE

$$\begin{aligned} E_i &= \langle (e_{n,i})^2 \rangle = \langle [s_e(nT + iT') - s_c(nT + iT')]^2 \rangle \\ &= \langle [\mathbf{a}_n^T (\mathbf{r}_{1i} - \mathbf{c}_i) + \mathbf{b}_n^T (\mathbf{r}_{2i} - \mathbf{d}_i) + \xi_{n,i}]^2 \rangle, \end{aligned} \tag{13}$$

where $\langle \cdot \rangle$ denotes the expectation of the quantity inside the brackets. Note that E_i cannot be smaller than the irreducible noise $\langle \xi_{n,i}^2 \rangle$.

The Minimum MSE (MMSE) is achieved when the N_i complex tap coefficients of the ith subcanceler are equal to the corresponding subchannel complex sampled values. The MMSE is given by

$$\min E_i = A \sum_{k>N_i} [r_1^2(kT + iT') + r_2^2(kT + iT')] + \langle \xi_i^2 \rangle, \tag{14}$$

where the data-symbol power is given by $A = \langle a^2 \rangle = \langle b^2 \rangle$.

This MMSE is obviously not the same for all the subcancelers. The adjustment algorithms for the updating of the subcanceler tap coefficients are obtained by taking the gradient of the MSE in (13) with respect to the tap vectors $\mathbf{c}_i$ and $\mathbf{d}_i$

$$\frac{\partial E_i}{\partial \mathbf{c}_i} = -2\langle \mathbf{a}_n e_{n,i} \rangle = \mathbf{r}_{1i} - \mathbf{c}_i \tag{15}$$

$$\frac{\partial E_i}{\partial \mathbf{d}_i} = -2\langle \mathbf{b}_n e_{n,i} \rangle = \mathbf{r}_{2i} - \mathbf{d}_i. \tag{16}$$

As is usual in practice, the gradients, with respect to the squared error rather than the MSE, are used for the adjustment of the tap coefficients. The corresponding stochastic tap adjustment algorithms are then

$$\mathbf{c}_{n+1,i} = \mathbf{c}_{n,i} + \alpha \mathbf{a}_n e_{n,i} \tag{17}$$

$$\mathbf{d}_{n+1,i} = \mathbf{d}_{n,i} + \alpha \mathbf{b}_n e_{n,i}, \tag{18}$$

where α is the step size of the adjustments and $i = 0, 1, \cdots, L - 1$.

Inspection of (11), (17), and (18) shows that each subcanceler requires a total of about $4N$ multiplications and additions for the filtering and updating operations. Therefore the implementation of the whole canceler requires $4LN$ multiplications and additions per symbol period. An analysis similar to those given in Refs. 4, 6, and 14 can be used to study the convergence properties of the MSE as a function of time. As is usually the case, the analysis assumes that the data vectors $\mathbf{a}_n$ and $\mathbf{b}_n$ in the subcancelers are uncorrelated between successive tap adjustments. Under these conditions it is shown in Appendix A that the MSE decreases as

$$\langle e_{n,i}^2 \rangle = (1 - 2\alpha A + 2\alpha^2 N_i A^2)^n \langle e_{0,i}^2 \rangle + \frac{1 - (1 - 2\alpha A + 2\alpha^2 N_i A^2)^n}{1 - (1 - 2\alpha A + 2\alpha^2 N_i A^2)} \cdot 2\alpha A \langle \xi_{n,i}^2 \rangle, \tag{19}$$

where N_i is the number of complex taps in the ith subcanceler.

In the derivation of (19) it was assumed that the first term on the right in (14) was zero. That is, it was assumed that the canceler was long enough to cover the memory span of the echo channel, and that no degradation was introduced by the finite precision in the digital implementation. Effects of finite precision are studied in detail in Ref. 2.

For the expression in (19) to converge, we require

$$|1 - 2\alpha A + 2\alpha^2 N_i A^2| < 1 \tag{20}$$

so that the step size α has to satisfy

$$0 < \alpha < \frac{1}{N_i A}. \tag{21}$$

The step size that provides the fastest speed of convergence to the corresponding steady-state MSE is obtained by setting the derivative of the expression in (20) to zero, i.e.,

$$\alpha_{\text{opt}} = \frac{1}{2N_i A}, \tag{22}$$

or one-half the maximum step size. From (19) it is clear that the ith subcanceler's steady-state MSE for a given step size is given by

$$\langle e_{\infty,i}^2 \rangle = \frac{\langle \xi_i^2 \rangle}{1 - \alpha N_i A}, \tag{23}$$

and the overall steady-state MSE averaged over a symbol period is

$$\langle e_{\infty}^2 \rangle = \frac{1}{L} \sum_{i=0}^{L-1} \frac{\langle \xi_i^2 \rangle}{1 - \alpha N_i A}. \tag{24}$$

If we assume that all the subcancelers have the same number N of complex taps and if we define

$$\langle \xi^2 \rangle = \frac{1}{L} \sum_{i=0}^{L-1} \langle \xi_i^2 \rangle \tag{25}$$

as the average power of the interfering signal in a symbol period, we can rewrite (24) in the form

$$E \equiv \langle e_\infty^2 \rangle = \frac{\langle \xi^2 \rangle}{1 - \alpha NA}. \tag{26}$$

The signal-to-noise ratio (s/n) achievable in front of the receiver can be derived from (26). The uncorrelated term $\langle \xi^2 \rangle$ consists of the noise in the channel with power P_u and the far signal with power P_S. The residual MSE E is the sum of P_S and some interfering "noise", I, defined by

$$I = E - P_S = \frac{\alpha NAP_S + P_u}{1 - \alpha NA}. \tag{27}$$

The steady-state received signal-to-noise ratio is then

$$s/n \equiv \frac{P_S}{I} = \frac{1 - \alpha NA}{\alpha NA + P_u/P_s}. \tag{28}$$

Notice from (22) and (28) that the maximum achievable s/n is 0 dB when the optimum step size for speed of convergence is used, and the channel noise is assumed to be zero ($P_u = 0$). Although the noise in (22) through (28) is not Gaussian, this expression has proved to be very useful for predicting the echo canceler's performance for various design parameters. Notice that, in the absence of channel impairments other than noise, the s/n is *not* a function of the relative powers of the echo and the far signal before cancellation. This result, of course, is not valid in a finite precision environment.

IV. EFFECT OF PHASE JITTER AND DOUBLE-TALKING

The distant echo, which has propagated through carrier systems, is likely to exhibit phase jitter. A Quadrature Amplitude Modulation (QAM) signal with phase jitter is usually defined as the real part of

$$Z_0(t) = \sum_n A_n G_1(t - nT) e^{j(\omega_c t + \Phi(t))}, \tag{29}$$

where $\Phi(t)$ is the phase jitter.

This complex signal is generally not an analytic signal; however, for small enough $\Phi(t)$, it is a very good approximation to an analytic signal. If we assume $|\Phi(t)| \ll 1$, we can write

$$Z_0(t) = Z_1(t) e^{j\Phi(t)} \cong Z_1(t) \cdot [1 + j\Phi(t)], \tag{30}$$

where $Z_1(t)$ is the analytic signal of the jitter-free, but possibly otherwise distorted, QAM signal. Taking the real part of (33), we get

$$s_0(t) = s_1(t) - \tilde{s}_1(t) \cdot \Phi(t). \tag{31}$$

It can be easily shown that $s_1(t)$ and $\tilde{s}_1(t)$ are uncorrelated. Therefore the signal $\tilde{s}_1(t) \cdot \Phi(t)$ can be considered as uncorrelated noise that is added to the jitter-free QAM signal $s_1(t)$. The phase jitter $\Phi(t)$ is usually slowly time varying compared to the symbol rate, so that we can assume that it remains constant in a given symbol period, i.e.,

$$\Phi(nT + iT') \cong \Phi_n = \text{constant for given } n \text{ and } i = 0, i, (L-1).$$

Sampling the output signal (34) at time $nT + iT'$, squaring, and taking the average, we get

$$\langle s_0^2(nT + iT') \rangle = \langle s_1^2(nT + iT') \rangle + \langle \tilde{s}_1^2(nT + iT') \rangle \cdot \langle \Phi_n^2 \rangle. \tag{32}$$

If we define the average powers in a symbol period

$$P_0 \triangleq \frac{1}{L} \sum_{i=0}^{L-1} \langle s_0^2(nT + iT') \rangle \tag{33}$$

$$P_1 \triangleq \frac{1}{L} \sum_{i=0}^{L-1} \langle s_1^2(nT + iT') \rangle = \frac{1}{L} \sum_{i=0}^{L-1} \langle \tilde{s}_1^2(nT + iT') \rangle, \tag{34}$$

we can rewrite (36) as

$$P_0 = P_1(1 + \langle \Phi_n^2 \rangle). \tag{35}$$

Thus the power, P_0, of the far echo is generally time varying due to the term $\langle \Phi_n^2 \rangle$. However, it can be shown that the power, P_1, of the jitter-free echo is a constant provided that $L \geq 2$. The expression, (26), for the residual MSE after convergence of the canceler is repeated here as

$$E = \langle e_\infty^2 \rangle = \frac{\langle \xi^2 \rangle}{1 - \alpha NA}, \tag{36}$$

where $\langle \xi^2 \rangle$ is the average power in the uncorrelated interference signal. One of the components of $\langle \xi^2 \rangle$ is the quantity $P_1 \cdot \langle \Phi_n^2 \rangle$, which is due to the phase jitter, and another component is the desired information-bearing signal received from the other modem. The average power of this later signal, defined as in (33), will be denoted by P_s. There is, of course, the ever-present additive Gaussian noise, and there are some other uncorrelated components that will generally depend on the specific architecture of the system. The average power of all these signals will be denoted by P_u. Equation (36) can now be written as

$$E = \frac{P_s + P_1 \cdot \langle \Phi_n^2 \rangle + P_u}{1 - \alpha NA}. \tag{37}$$

This is the input power seen by the receiver after echo cancellation has taken place. The useful power for the receiver is P_s and the rest of the power is interfering "noise", I, defined by

$$I = E - P_s = \frac{\alpha NAP_s + P_1 \cdot \langle \Phi_n^2 \rangle + P_u}{1 - \alpha NA}. \tag{38}$$

The steady-state received s/n in a given symbol period is then

$$s/n = \frac{P_s}{I} = \frac{1 - \alpha NA}{\alpha NA + (P_1/P_s) \cdot \langle \Phi_n^2 \rangle + P_u/P_s}. \tag{39}$$

Notice that the s/n is now a function of the echo-to-signal ratio before cancellation. The phase jitter, $\Phi(t)$, is usually modeled as a slowly varying sine wave. As a consequence, the expression for the s/n is also time varying, and in order to compute the worst-case s/n, we have to use the largest value of $\langle \Phi_n^2 \rangle$ in (39). Assume that $\Phi(t)$ is a simple sine wave

$$\Phi(t) = C \cos 2\pi f_0 t. \tag{40}$$

If B is the peak-to-peak phase jitter in degrees, then the maximum value of $\langle \Phi_n^2 \rangle$ is

$$\max \langle \Phi_n^2 \rangle = C^2 = \left(\frac{\pi}{360} B \right)^2. \tag{41}$$

This expression does not depend on frequency and can be used even if the jitter cannot be modeled as a sine wave. However, if we want to check experimental results against analytical results, we have to use the time average of $\langle \Phi_n^2 \rangle$, since laboratory equipment will generally average power measurements over long periods of time. In this case the quantity

$$\langle \Phi_n^2 \rangle = \frac{C^2}{2} = \frac{1}{2} \left(\frac{\pi}{360} B \right)^2 \tag{42}$$

should be used in (39).

V. EFFECT OF FREQUENCY OFFSET

The analytic signal of a QAM signal affected by frequency offset can be represented by

$$Z_0(t) = \sum_n A_n G_1(t - nT) e^{j(\omega_c t + \omega_1 t)}, \tag{43}$$

where ω_1 is the radian frequency offset. Frequency offset can be considered as a special case of phase-jitter if we replace $\Phi(t)$ in (29) by $\omega_1 t$. However, the expansion (30) does not hold anymore, even for a very small ω_1. In order to study the effect of frequency offset on the

in-band canceler we can use the analysis given in Section III and rewrite (43) in the following way:

$$Z_0(t) = \sum_n A'_n R_1(t - nT), \tag{44}$$

where, if we assume $\omega_c T = k2\pi$,

$$A'_n = A_n e^{j\omega_1 nT} \tag{45}$$

and $R_1(t)$ consists of in-phase and quadrature bandpass filters. The sampled output of the ith subchannel is, from (12),

$$s_e(nT + iT') = \mathbf{a}'^T_n \mathbf{r}_{1i} + \mathbf{b}'^T_n \mathbf{r}_{2i}, \tag{46}$$

where we assume, for the time being, that $\xi_{n,i} = 0$.

If we define

$$\mathbf{A}_n = \mathbf{a}_n + \mathbf{j}\mathbf{b}_n \quad \text{and} \quad \mathbf{R}_{1i} = \mathbf{r}_{1i} + \mathbf{j}\mathbf{r}_{2i}, \tag{47}$$

we can rewrite (46) in the two following ways:

$$\begin{aligned} 2s_e(nT + iT') &= (e^{jn\Delta}\mathbf{A}^T_n)\cdot\mathbf{R}^*_{1i} + \mathbf{R}^T_{1i}\cdot(e^{jn\Delta}\mathbf{A}_n)^* \\ &= \mathbf{A}^T_n\cdot(e^{-jn\Delta}\mathbf{R}_{1i})^* + (e^{-jn\Delta}\mathbf{R}^T_{1i})\cdot\mathbf{A}^*_n, \end{aligned} \tag{48}$$

where we have defined $\omega_1 T = \Delta$, and * denotes the complex conjugate.

The two expressions in (48) lead to two different interpretations of the effect of frequency offset on a QAM signal. First we can consider that the symbol vectors $\mathbf{A}_n$ are rotated by small increments Δ at the input of a time-invariant channel. Alternatively we can assume that the vectors $\mathbf{A}_n$ are the channel's inputs and that the sampled channel's impulse responses $\mathbf{R}_{1i}$ are rotated by increments—Δ. The canceler's performance in the presence of frequency offset is studied in Appendix B, where we have assumed that the nonrotated symbols $\mathbf{A}_n$ are the inputs of both the canceler and the channel, and that the algorithms given in Section III are used for updating the tap coefficients. Under these conditions it is shown that the mean steady-state tap coefficients satisfy

$$\langle \mathbf{C}_{n,i} \rangle = \mathbf{R}_{1i} e^{-jn\Delta} \frac{\alpha A e^{j\Delta}}{1 - (1 - \alpha A)e^{j\Delta}}. \tag{49}$$

The quantity on the right is equal to the ith subchannel's complex impulse response at time $(nT + iT')$ multiplied by a constant complex number. Therefore, the canceler's complex taps rotate and track the channel's complex impulse response with a fixed phase lag and a different amplitude. It is interesting to note that the mean-tap values go to zero when the step size α goes to zero. This most peculiar behavior was also observed experimentally. The ith subcanceler's steady-state MSE after cancellation is derived in Appendix B. It is given by

$$\langle e_{n,i}^2 \rangle = \langle e_{n,i}^2(\Delta = 0) \rangle + \frac{1 - \alpha A}{1 - \alpha NA} \cdot \frac{A\Delta^2}{\alpha^2 A^2 + (1 - \alpha A)\Delta^2} \cdot \mathbf{R}_{1i}^T \mathbf{R}_{1i}^*, \quad (50)$$

where $\langle e_{n,i}^2(\Delta = 0) \rangle$ is the MSE in the absence of frequency offset.

The MSE for the whole canceler is obtained by averaging (50) over all the subcancelers. The resulting quantity is not very useful, because it is dependent on the channel characteristics. This is not the case for the Echo-Return-Loss Enhancement (ERLE), which is also studied in Appendix B. The ERLE is defined as the ratio between the power of the uncanceled echo and the power of the residual echo. It is given by

$$\text{ERLE} = -10 \log \left(\frac{1 - \alpha A}{1 - \alpha NA} \cdot \frac{\Delta^2}{\alpha^2 A^2 + (1 - \alpha A)\Delta^2} \right). \quad (51)$$

This expression is the same for all the subcancelers, and therefore it gives also the ERLE for the whole canceler. In the derivation of (51) it was assumed that there was no interfering, uncorrelated signal at the output of the channel.

VI. EXPERIMENTAL RESULTS

Experimental results were obtained by using an in-band data-driven echo canceler implemented on a bit-slice processor. Figure 4 shows

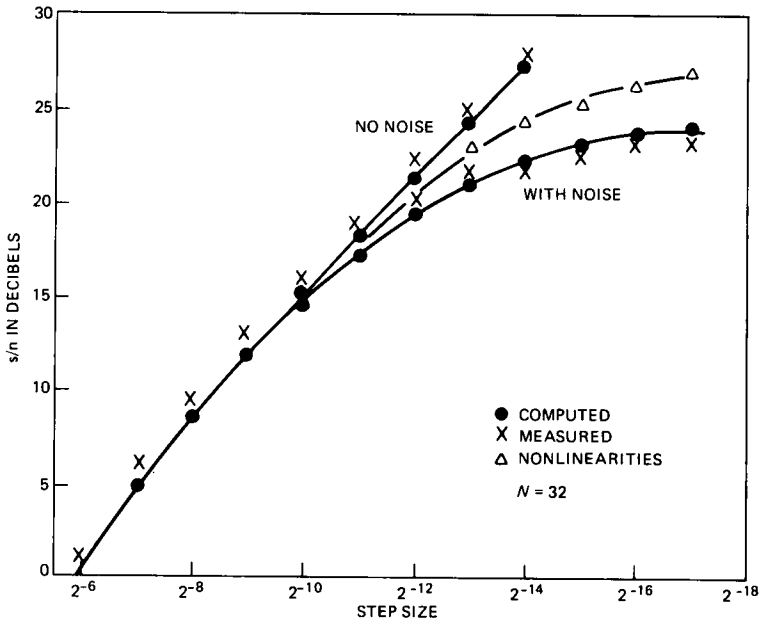

Fig. 4—The s/n in the presence of noise or nonlinearities.

performance curves giving the achievable s/n as a function of the step size for various types of channel impairments. A simulated far signal was added to the echo before cancellation, and the s/n was measured after cancellation (point A in Fig. 1b). The echo and the far signal had the same power before cancellation. The straight curve corresponds to the case where no impairments, other than linear distortion, were present in the echo channel. Notice that the achievable s/n, under these ideal conditions, increases by 3 dB when the step size decreases by a factor of two. One of the two curves that flatten out was obtained by adding noise to the echo and the far signal. In this case the noise power was 24 dB below the echo power. As one might expect, this curve goes asymptotically to an s/n of 24 dB when the step size becomes small. In both the preceding cases the theoretical curves were computed by using (28). The third curve was obtained by introducing nonlinearities in the echo channel. The amount of nonlinearities used in this experiment corresponded to the worst case reported in the 1969–70 DDD connection survey.[15]

Figure 5 shows similar results when phase jitter was introduced in the echo channel. The theoretical curves were obtained by using (39) and (42). The frequency of the phase jitter used in the experiments was 120 Hz, and the far signal and far echo had again the same power. If the far echo's power were X dB below the power of the far signal, then the flat portion of the curves would move up by X dB, as seen

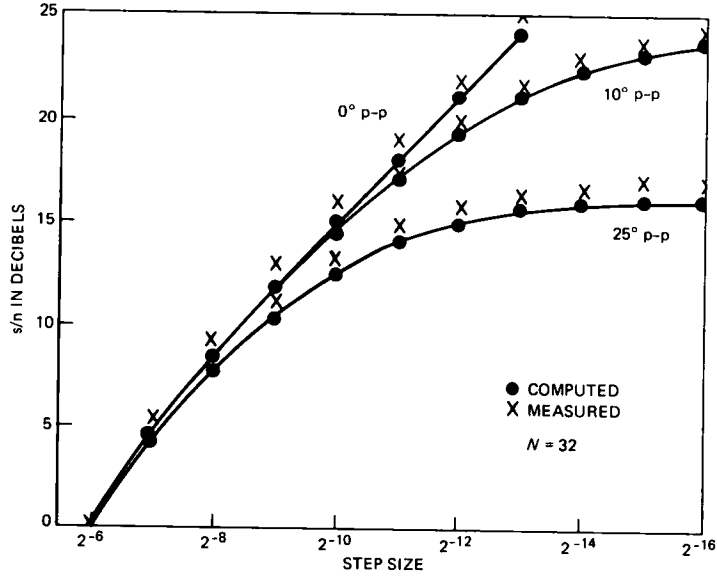

Fig. 5—The s/n degradation due to phase jitter.

from (39). A word of caution is in order here about the usage of all the results discussed so far for predicting receiver performance. The noise in the s/n is not Gaussian, and, thus, standard probability of error formulas assuming Gaussian noise should not be used in a naive way. However, we found that the preceding results were very good indicators for predicting relative receiver performance for various design parameters and channel impairments. One has also to consider that the residual echo is amplitude modulated by the phase jitter when this impairment is present in the echo channel, as seen from (31) and Fig. 6. The probability of error, in this case will be mostly influenced by the maxima of the residual echo, rather than by its average power.

Figures 7 and 8 show experimental results obtained when frequency offset was present in the echo channel. The Echo-Return-Loss Enhancement (ERLE) shown in Fig. 7 is defined as the ratio between the echo power before cancellation and the power of the residual echo after cancellation. No double-talker was present in these experiments.

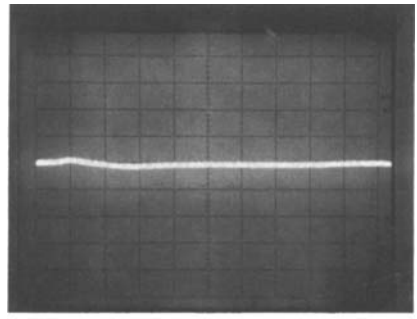

(a)

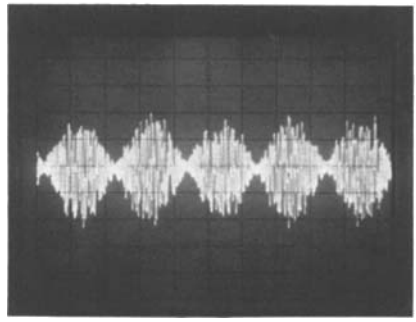

(b)

Fig. 6—Residual mean-squared error (a) without phase jitter and (b) in the presence of phase jitter.

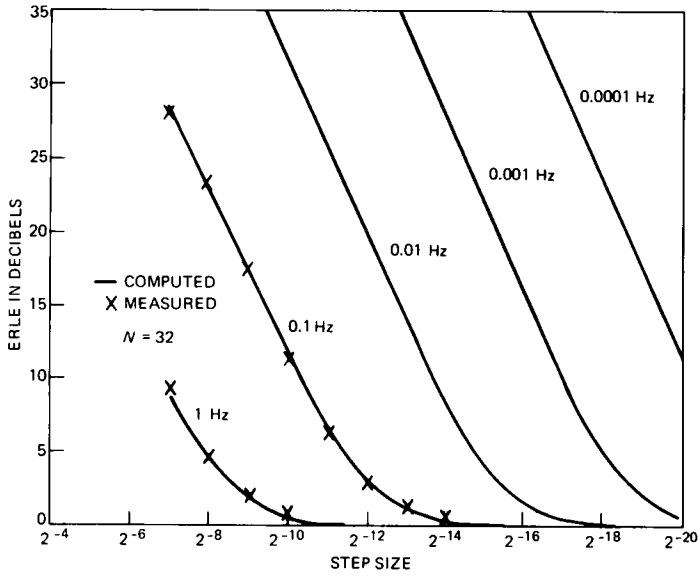

Fig. 7—ERLE degradation due to frequency offset.

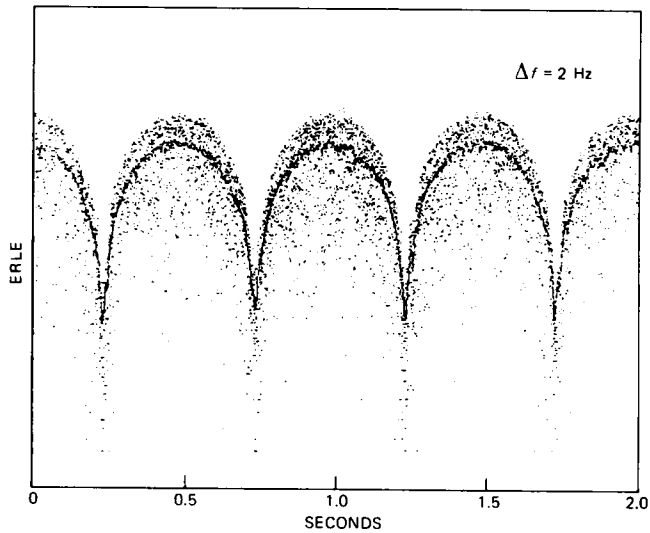

Fig. 8—Evolution of the ERLE in the presence of frequency offset and with frozen taps.

The theoretical curves were computed by using (51). The agreement between the experimental and analytical results is seen to be excellent. Notice the intuitively satisfying result that the tracking capability of the echo canceler improves with large step sizes. Figure 7 was obtained

by conducting the following experiment. The echo canceler was first converged when no frequency offset was present in the echo channel. The canceler's taps were then frozen and a frequency offset of 2 Hz was introduced in the channel. Notice the periodic evolution of the ERLE. As was mentioned in the preceding section, the effect of frequency offset can be modeled by a periodic rotation of the sampled values of the in-phase and quadrature impulse responses of the echo channel. Thus, the ERLE will pass through a minimum when these sampled values are in phase with the complex tap coefficients of the echo canceler. It will pass through a maximum when the sampled impulse responses and the complex tap coefficients are out of phase by 180 degrees.

We conclude this section with some brief comments on the implications of the preceding results on the practical implementation of high-speed, full-duplex DDD modems. The effects of noise, nonlinearities, and phase jitter are very similar, as seen in Figs. 4, 5, and 7. In each case a comfortable s/n can be achieved by using a small enough step size in the tap adjustment algorithm. This is certainly true for the 4800 b/s modem described in Ref. 1 that requires an s/n of about 14 dB in order to achieve a bit-error rate of 10^{-5}. It is usually assumed that the far echo is always at least 10 dB below the far signal. Thus, under these worst-case conditions, the flat portions of the curves in Fig. 5 would all move up by 10 dB. In this case, even a 25-degree peak-to-peak phase jitter in the far echo would not deteriorate significantly the canceler's performance, provided that the step size is chosen small enough. On the other hand, a small step size will limit the echo canceler's capability of tracking frequency offset in the far echo, as shown in Fig. 7. A frequency offset as small as 0.01 Hz can seriously degrade the echo canceler's performance. It is generally accepted that the United States' domestic network does not introduce frequency offset in the far echo. However, this is not necessarily true in other countries. Frequency offset compensation techniques are known, but they are quite expensive to implement.[4,11]

REFERENCES

1. J. J. Werner, "An Echo-Cancellation-Based 4800 bps Full-Duplex DDD Modem," IEEE J. Selected Areas Commun., *SAC-2*, No. 5 (September 1984), pp. 722–30.
2. J. M. Cioffi and J. J. Werner, "The Effect of Biases on Digitally Implemented Data-Driven Echo Cancelers," AT&T Tech. J., this issue.
3. V. G. Koll and S. B. Weinstein, "Simultaneous Two-Way Data Transmission Over a Two-Wire Circuit," IEEE Trans. Commun., *COM-21*, No. 2 (February 1973), pp. 143–7.
4. K. H. Mueller, "A New Digital Echo Canceller for Two-Wire Full-Duplex Data Transmission," IEEE Trans. Commun., *COM-24*, No. 9 (September 1976), pp. 956–67.
5. D. D. Falconer, K. H. Mueller, and S. B. Weinstein, "Echo Cancellation Techniques for Full-Duplex Data Transmission on Two-Wire Lines," Proc. NTC, Dallas, December 1976.

6. S. B. Weinstein, "A Passband Data-Driven Echo Canceller for Full-Duplex Transmission on Two-Wire Circuits," IEEE Trans. Commun. (July 1977), pp. 654–66.
7. J. R. Rosenberger and E. J. Thomas, "Performance of an Adaptive Echo Canceller in a Noisy, Linear, Time Invariant Environment," B.S.T.J., *50*, No. 3 (March 1971), pp. 785–813.
8. E. J. Thomas, "An Adaptive Echo Canceller in a Non-Ideal Environment (Nonlinear or Time Variant)," B.S.T.J., *50*, No. 8 (October 1971), pp. 2779–95.
9. H. G. Suyderhoud and M. Onufry, "Performance of a Digital Adaptive Echo Canceller in a Simulated Satellite Circuit Environment," AIAA 4th Commun. Satellite Syst. Conf., Washington, April 24–26, 1972.
10. R. D. Gitlin and S. B. Weinstein, "The Effects of Large Interference on the Tracking Capability of Digitally Implemented Echo Cancellers," IEEE Trans. Commun., *COM-26*, No. 6 (June 1978), pp. 833–9.
11. R. D. Gitlin and J. S. Thompson, "A Phase Adaptive Structure for Echo Cancellation," IEEE Trans. Commun., *COM-26*, No. 8 (August 1978), pp. 1211–20.
12. D. D. Falconer, "Adaptive Reference Echo Cancellation," IEEE Trans. Commun. (September 1982), pp. 2083–94.
13. J. J. Werner, "Modulated Passband Signal Generator," U.S. Patent No. 4,015,222, March 29, 1977.
14. N. A. M. Verhoecks et al., "Digital Echo Cancellation for Baseband Data Transmission," IEEE Trans. Acoust., Speech, Signal Processing, *ASSP-27*, No. 6 (December 1979), pp. 768–81.
15. F. P. Duffy and T. W. Thatcher, Jr., "Analog Transmission Performance on the Switched Telecommunications Network," B.S.T.J., *50*, No. 4 (April 1971), pp. 1311–48.

APPENDIX A

Convergence of the MSE

For notational convenience we will delete the index i in the equations but it will be understood that the analysis applies to a subcanceler and not the whole canceler. The updating algorithms are, from (19) and (20),

$$\mathbf{c}_{n+1} = \mathbf{c}_n + \alpha \mathbf{a}_n e_n \tag{52}$$

$$\mathbf{d}_{n+1} = \mathbf{d}_n + \alpha \mathbf{b}_n e_n. \tag{53}$$

If we define the complex tap weights and data symbols

$$\mathbf{C}_n \triangleq \mathbf{c}_n + j\mathbf{d}_n \tag{54}$$

$$\mathbf{A}_n \triangleq \mathbf{a}_n + j\mathbf{b}_n, \tag{55}$$

we can rewrite (52) and (53) in the compact form

$$\mathbf{C}_{n+1} = \mathbf{C}_n + \alpha \mathbf{A}_n e_n. \tag{56}$$

Subtracting both sides of (56) from the complex vector

$$\mathbf{R} = \mathbf{r}_1 + j\mathbf{r}_2, \tag{57}$$

we get the impulse-response error signal

$$\epsilon_{n+1} = \epsilon_n - \alpha \mathbf{A}_n e_n + \mathbf{F}_n, \tag{58}$$

where we have defined the canceler tap errors as

$$\epsilon_n \triangleq \mathbf{R} - \mathbf{C}_n = [\mathbf{r}_1 - \mathbf{c}_n + j(\mathbf{r}_2 - \mathbf{d}_n)]. \tag{59}$$

In (58) we have also included a complex vector $\mathbf{F}_n$, which will be needed in Appendix B, to account for frequency offset. In this Appendix this quantity is taken to be zero.

The canceler error at the nth iteration is, from (13),

$$e_n = (\mathbf{r}_1^T - \mathbf{c}_n^T)\mathbf{a}_n + (\mathbf{r}_2^T - \mathbf{d}_n^T)\mathbf{b}_n + \xi_n \tag{60}$$

$$= \frac{1}{2}(\boldsymbol{\epsilon}_n^T\mathbf{A}_n^* + \mathbf{A}_n^T\boldsymbol{\epsilon}_n^*) + \xi_n, \tag{61}$$

where the asterisk * denotes the complex conjugate. The MSE at the nth iteration becomes

$$\langle e_n^2\rangle = \frac{1}{4}\langle(\boldsymbol{\epsilon}_n^T\mathbf{A}_n^* + \mathbf{A}_n^T\boldsymbol{\epsilon}_n^*)^2\rangle + \langle\xi_n^2\rangle. \tag{62}$$

The tap error vectors $\boldsymbol{\epsilon}_n$ depend only on the vectors $\mathbf{A}_{n-1}$ as shown in (58). If we assume that consecutive data vectors $\mathbf{A}_{n-1}$ and $\mathbf{A}_n$ are uncorrelated, and that the $a_n's$ are uncorrelated with the $b_n's$, we can rewrite (62) as

$$\langle e_n^2\rangle = A\langle\boldsymbol{\epsilon}_n^T\boldsymbol{\epsilon}_n^*\rangle + \langle\xi_n^2\rangle, \tag{63}$$

where $A = \langle a_n^2\rangle = \langle b_n^2\rangle$ is the variance in the symbols. The MSE at the $(n+1)$th iteration is

$$\langle e_{n+1}^2\rangle = A\langle\boldsymbol{\epsilon}_{n+1}^T\boldsymbol{\epsilon}_{n+1}^*\rangle + \langle\xi^2\rangle. \tag{64}$$

Using (58), we get

$$\langle e_{n+1}^2\rangle = A\langle(\boldsymbol{\epsilon}_n^T + \mathbf{F}_n^T - \alpha e_n\mathbf{A}_n^T) \cdot(\boldsymbol{\epsilon}_n^* + \mathbf{F}_n^* - \alpha e_n\mathbf{A}_n^*)\rangle + \langle\xi^2\rangle \tag{65}$$

$$= A\langle\boldsymbol{\epsilon}_n^T\boldsymbol{\epsilon}_n^*\rangle - \alpha A\langle e_n(\mathbf{A}_n^T\boldsymbol{\epsilon}_n^* + \boldsymbol{\epsilon}_n^T\mathbf{A}_n^*)\rangle + 2\alpha^2A^2N\langle\boldsymbol{\epsilon}_n^2\rangle + Af(\mathbf{F}_n), \tag{66}$$

where we have used

$$\mathbf{A}_n^T\mathbf{A}_n^* = 2AN, \tag{67}$$

and have defined

$$f(\mathbf{F}_n) = \langle\mathbf{F}_n^T(\boldsymbol{\epsilon}_n^* - \alpha e_n\mathbf{A}_n^*) + (\boldsymbol{\epsilon}_n^T - \alpha e_n\mathbf{A}_n^T)\mathbf{F}_n^*\rangle. \tag{68}$$

Setting $\mathbf{F}_n$ to zero and using (61) and (63) in (66), we get the equation

$$\langle e_{n+1}^2\rangle = (1 - 2\alpha A + 2\alpha^2NA^2)\cdot\langle e_n^2\rangle + 2\alpha A\langle\xi^2\rangle. \tag{69}$$

The solution to this recurrence equation is

$$\langle e_n^2\rangle = (1 - 2\alpha A + 2\alpha^2NA^2)^n\langle e_0^2\rangle + \frac{1 - (1 - 2\alpha A + 2\alpha^2NA^2)^n}{1 - (1 - 2\alpha A + 2\alpha^2NA^2)}\cdot 2\alpha A\langle\xi^2\rangle. \tag{70}$$

APPENDIX B

Effect of Frequency Offset

It was shown in Section VI that the effect of frequency offset can be accounted for by rotating the channel's sampled impulse responses at the symbol rate by angles $\Delta = \omega_1 T$, where ω_1 is the radian frequency offset. We can then rewrite (56) in the following way:

$$\mathbf{R}_{n+1} - \mathbf{C}_{n+1} = \mathbf{R}_n - \mathbf{C}_n - \alpha \mathbf{A}_n e_n + \mathbf{R}_{n+1} - \mathbf{R}_n \tag{71}$$

$$\boldsymbol{\epsilon}_{n+1} = \boldsymbol{\epsilon}_n - \alpha \mathbf{A}_n e_n + \mathbf{F}_n, \tag{72}$$

where we have defined

$$\boldsymbol{\epsilon}_n = \mathbf{R}_n - \mathbf{C}_n = \mathbf{R} e^{-jn\Delta} - \mathbf{C}_n \tag{73}$$

$$\mathbf{F}_n = \mathbf{R}_{n+1} - \mathbf{R}_n = \mathbf{R} e^{-jn\Delta}(e^{-j\Delta} - 1). \tag{74}$$

The analysis given in Appendix A can now be carried through up to (69) by keeping $\mathbf{F}_n$ different from zero. The MSE at the $(n+1)$th iteration is now

$$\langle e_{n+1}^2 \rangle = (1 - 2\alpha A + 2\alpha^2 N A^2)\langle e_n^2 \rangle + 2\alpha A \langle \xi^2 \rangle + A f(\mathbf{F}_n), \tag{75}$$

where from (68)

$$f(\mathbf{F}_n) = \langle \mathbf{F}_n^T(\boldsymbol{\epsilon}_n^* - \alpha e_n \mathbf{A}_n^*) + (\boldsymbol{\epsilon}_n^T - \alpha e_n \mathbf{A}_n^T)\mathbf{F}_n^* \rangle. \tag{76}$$

Using (72) and (73), we can rewrite this expression in the following way:

$$f(\mathbf{F}_n) = \mathbf{F}_n^T(\mathbf{R}_n^* - \langle \mathbf{C}_{n+1}^* \rangle) + (\mathbf{R}_n^T - \langle \mathbf{C}_{n+1}^T \rangle)\mathbf{F}_n^*. \tag{77}$$

The evaluation of this quantity requires the knowledge of the mean-tap fluctuations $\langle \mathbf{C}_n \rangle$. Replacing e_n in (56) by its value in (61) and taking the average gives

$$\begin{aligned} \langle \mathbf{C}_{n+1} \rangle &= \langle \mathbf{C}_n \rangle + \frac{\alpha}{2} \langle \mathbf{A}_n(\boldsymbol{\epsilon}_n^T \mathbf{A}_n^* + \mathbf{A}_n^T \boldsymbol{\epsilon}_n^*) \rangle \\ &= \langle \mathbf{C}_n \rangle + \alpha A \langle \boldsymbol{\epsilon}_n \rangle. \end{aligned} \tag{78}$$

From (73) we get

$$\langle \mathbf{C}_{n+1} \rangle = \langle \mathbf{C}_n \rangle (1 - \alpha A) + \alpha A \mathbf{R} e^{-jn\Delta}. \tag{79}$$

After some algebra, the solution of this recurrence equation is found to be

$$\langle \mathbf{C}_{n+1} \rangle = \langle \mathbf{C}_0 \rangle (1 - \alpha A)^{n+1} + \alpha A \mathbf{R} e^{-jn\Delta} \cdot \frac{1 - (1 - \alpha A)^{n+1} e^{j(n+1)\Delta}}{1 - (1 - \alpha A) e^{j\Delta}}. \tag{80}$$

In steady-state operation, as n goes to infinity, we have

$$\langle \mathbf{C}_{n+1} \rangle = \alpha A \mathbf{R} e^{-jn\Delta} \cdot \frac{1}{1 - (1 - \alpha A)e^{j\Delta}}. \tag{81}$$

We can now get an expression for the steady-state value of $f(\mathbf{F}_n)$ in (77). After some algebra

$$f(\mathbf{F}_n) = -2R^2(1 - \alpha A) \cdot \frac{3 - 4\cos\Delta + \cos 2\Delta - 2\alpha A(1 - \cos\Delta)}{1 + (1 - \alpha A)^2 - 2(1 - \alpha A)\cos\Delta}, \tag{82}$$

where we have defined

$$R^2 = \mathbf{R}^T \mathbf{R}^*. \tag{83}$$

In the usual case where $\Delta \ll 1$, we can use the approximation

$$\cos\Delta \cong 1 - \frac{\Delta^2}{2} \tag{84}$$

in which case (82) simplifies to

$$f(\mathbf{F}_n) \cong \frac{2\alpha A \Delta^2 (1 - \alpha A) \cdot R^2}{\alpha^2 A^2 + (1 - \alpha A)\Delta^2}. \tag{85}$$

This quantity is a constant, which does not depend on time. The solution to the recurrence (75) is then, in steady-state operation,

$$\langle e_n^2 \rangle = \langle e_n^2(\Delta = 0) \rangle + \frac{1 - \alpha A}{1 - \alpha NA} \cdot \frac{A\Delta^2 R^2}{\alpha^2 A^2 + (1 - \alpha A)\Delta^2}, \tag{86}$$

where $\langle e_n^2(\Delta = 0) \rangle$ designates the steady-state value of the MSE given in (70) in the absence of frequency offset.

We can use this expression to find the value of the ERLE in the presence of frequency offset. We will assume that there is no other impairment in the channel. The output of the channel is then

$$s_{e,n} = \frac{1}{2}(\mathbf{A}_n^T \mathbf{R}_n^* + \mathbf{R}_n^T \mathbf{A}_n^*), \tag{87}$$

and the mean-squared output of the channel is

$$\langle s_{e,n}^2 \rangle = A \mathbf{R}_n^T \mathbf{R}_n^* = AR^2. \tag{88}$$

The MSE after cancellation is given in (86), where we put the first term on the right equal to zero. The ERLE is then

$$\begin{aligned} \text{ERLE} &= 10 \log\langle s_{e,n}^2 \rangle - 10 \log\langle e_n^2 \rangle \\ &= -10 \log \left(\frac{1 - \alpha A}{1 - \alpha NA} \cdot \frac{\Delta^2}{\alpha^2 A^2 + (1 - \alpha A)\Delta^2} \right). \end{aligned}$$

Notice that the ERLE goes to zero when the step size α goes to zero.

AUTHOR

Jean-Jacques Werner, Ing. Deg., 1965, INSA, Lyon, France; M.S. (Electrical Engineering), 1967, Laval University, Canada; Eng. Sc.D. (Electrical Engineering), 1973, Columbia University; Bell Laboratories, 1973–1982; AT&T Information Systems, 1983—. At Bell Laboratories and AT&T Information Systems, Mr. Werner has worked on problems in data transmission and digital signal processing. Member, Sigma Xi, IEEE.